Journal of Alloys and Compounds 509 (2011) 4478–4483

Contents lists available at ScienceDirect

Journal of Alloys and Compounds

journal homepage: www.elsevier.com/locate/jallcom

Physical properties of Gd_7NiPd_2 single crystal

M. Oboz*, E. Talik, J. Kusz, A. Winiarski

Institute of Physics, University of Silesia, Uniwersytecka 4, 40 007 Katowice, Poland

ARTICLE INFO

Article history:
Received 18 November 2010
Received in revised form 3 January 2011
Accepted 4 January 2011
Available online 22 January 2011

Keywords:
Rare-earth alloys and compounds
Crystal growth
Anisotropy
Magnetocaloric

ABSTRACT

Investigations of X-ray diffraction, electronic structure, *dc*-magnetization *M*(T), *ac*-magnetic susceptibility χ_{ac}(T) and magnetocaloric properties for the Gd_7NiPd_2 single crystal were performed. A single crystal of Gd_7NiPd_2 was grown by the Czochralski method from a levitating melt. Anomalies in χ_{ac}(T) and *M*(T)-curves establish that Gd_7NiPd_2 undergoes a long-range ferromagnetic-type ordering at T_C = 298 K, followed by a spin-reorientation below 135 K. The magnetization data indicate that there is an excess magnetic moment calculated per Gd^{3+} ions. The measured XPS valence band indicates the hybridization effect between Gd 5*d*, Ni 3*d* and Pd 4*d* states. The calculated values of entropy change ΔSm for the examined compound amount to −6.85 J/K kg for the *a*-axis and −6.49 for the *c*-axis at 7 T.

1. Introduction

Materials based on gadolinium are prospective for applications in magnetic refrigeration cycles. Recently, magnetic materials with relatively high Curie temperatures (T_C) are researched as potential candidates for magnetic refrigeration if they show large enough magnetocaloric effect (MCE). Several intermetallics based on rare earth and transition metals show interesting magnetocaloric properties [1–4]. However, their ordering temperatures are very often below room temperature. Preliminary examination of the crystal structure, magnetic and electrical behaviour of $Gd_{7-x}Y_xPd_3$ (x = 0, 1, 2, 3, 4, 5, 6) single crystals were performed [5–9]. Single crystals of solid solutions $Gd_{7-x}Y_xPd_3$ were reported to crystallize in the same structure as the parent Gd_7Pd_3 compound [5–9]. In spite of yttrium substitution crystal structure was stable. With increasing Y-content the ferromagnetic transition shifts down to lower temperatures, whereas Gd_7Pd_3 orders ferromagnetically below 334 K; Gd_6YPd_3, $Gd_5Y_2Pd_3$ and $Gd_3Y_4Pd_3$ undergo magnetic transformation at 299, 263 and 197 K, respectively.

As a part of current research concerning the development of new magnets for magnetic refrigeration devices we characterised the Gd_7NiPd_2 single crystal. This paper presents results of the crystal and electronic structure, magnetic and magnetocaloric properties investigations of a new Gd_7NiPd_2 compound.

2. Experimental

The single crystal of Gd_7NiPd_2 was grown by the Czochralski method from a levitated melt using high purity starting materials [10].

The real structure of the as-grown crystal was examined by the Berg–Barrett topography using Fe K_α radiation. The sensitivity of the method to the misorientation is ~1′. X-ray reflections from (h k l) planes were recorded in the range of 2Θ in the range 70–100° on Agfa-Gevaert Structurix D2 film, which was placed close to the crystal surface. The distance between the crystal and the film was about 1 mm to obtain a good pattern. These examinations were performed to check the quality of the obtained single crystals. The spatial resolution was 10 μm.

Single crystal X-ray diffraction was performed at room temperature on a four-circle KM4 diffractometer using graphite-monochromatized Mo K_α radiation. The intensities of reflections were corrected for Lorentz and polarization effects.

XPS spectra of the above single crystal were measured with monochromatized Al K_α radiation (1486.6 eV) at room temperature using a PHI 5700 ESCA spectrometer. The energy spectra were determined by a hemispherical mirror analyzer with an energy resolution of about 0.3 eV.

Magnetization was measured using a Quantum Design MPMSXL-7AC SQUID magnetometer in the temperature range 2–400 K in magnetic fields up to 7 T. The *ac*-magnetic susceptibility was measured in the temperature range 2–400 K and at a frequency of 100 Hz.

3. Results and discussion

Fig. 1a shows a photo of "as-grown" Gd_7NiPd_2 single crystal. Fig. 1b presents a topographic Berg–Barrett X-ray image of the studied Gd_7NiPd_2 single crystal. This image indicates that the obtained single crystal was good quality without mosaic structure.

The crystal structure of the Gd_7NiPd_2 was refined by the full least squares method using the SHELX-97 [11]. The results of the structural refinements are collected in Table 1. The atomic coordinates, isotropic and anisotropic parameters are listed in Table 2. Apart from ascertaining the good single-crystalline quality of the sample, the X-ray diffraction data have showed that the Gd_7NiPd_2 compound crystallized in the hexagonal Th_7Fe_3-type structure with space group $P6_3mc$. From the tables one can recognize that in the unit cell of Gd_7NiPd_2 the gadolinium atoms occupy three non-equivalent crystallographic positions (2*b* and 6*c* sites) and the

* Corresponding author. Tel.: +48 32 359 1581; fax: +48 32 258 8431.
E-mail address: monika.oboz@us.edu.pl (M. Oboz).

0925-8388/$ – see front matter © 2011 Elsevier B.V. All rights reserved.
doi:10.1016/j.jallcom.2011.01.034

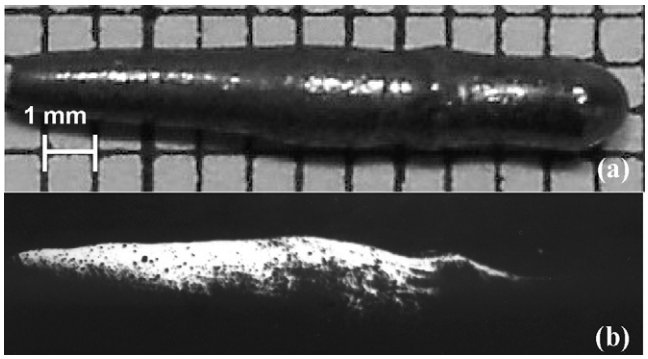

Fig. 1. Single crystal view of Gd_7NiPd_2: (a) "as grown" photo and (b) as Berg–Barrett topography.

Table 1
Crystal data and structure refinement for Gd_7NiPd_2.

Structure parameter	Room temperature data
Crystal system, space group	Hexagonal, $P6_3mc$
Unit cell dimensions	a = 9.9372(5) Å
	c = 6.2674(4) Å
Volume	536.0(1) Å^3
Absorption coefficient	23.78 mm^{-1}
F(0 0 0)	568.0
Theta range for data collection	4.02–34.64°
Reflections collected	6250
Goodness of fit	1.121
Final R indices [$I > 2\sigma(I)$]	R_1 = 0.0259, wR_2 = 0.0699
Extinction coefficient	0.0011(2)

Table 3
The lattice parameters of Gd_7NiPd_2 and Gd_7Pd_3.

Parameters			References
a [Å]	c [Å]	V [Å^3]	
Gd_7NiPd_2			
9.9372(5)1	6.2674(4)	536.0(1)	This work
1(6)			Single crystal (300 K)
Gd_7Pd_3			
9.981(1)	6.279(1)	541.7(2)	Single crystal (300 K) [6]

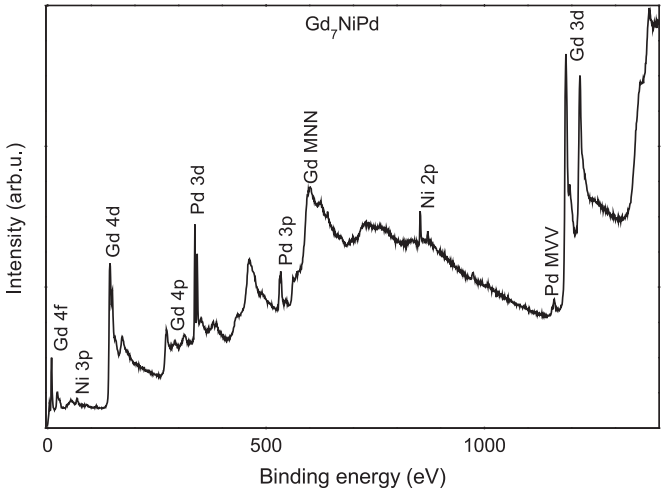

Fig. 2. XPS spectrum of a Gd_7NiPd_2 single crystal in the energy range 0–1400 eV.

Pd atoms share their sites with Ni atom (6c position). The X-ray measurements and the refinement of the crystal structure of the Gd_7NiPd_2 indicate that Ni gets substituted randomly by replacing Pd of the parent compound Gd_7Pd_3.

The determined lattice parameters of Gd_7NiPd_2 were a = 9.9372 Å and c = 6.2674 Å. The lattice parameters of the Gd_7NiPd_2 are smaller compare to the parent Gd_7Pd_3 compound [6] (Table 3). The atomic radius of the nickel is slightly lower than that of palladium (135 pm for Ni and 137 pm for Pd). So, the substitution of nickel should a little decrease the values of lattice parameters and the unit cell volume.

The XPS spectrum of the Gd_7NiPd_2 single crystal measured in a wide energy range (0–1400 eV) is shown in Fig. 2. The single crystal was very compact. So just after breaking its under UHV conditions, even for such sensitive to contamination materials, no carbon and almost no oxygen was found. The measured surface was clean enough and a good quality of spectra could be obtained. Using the XPS spectrum the stoichiometry was also checked. It was found to be in agreement with the nominal one.

The measured XPS valence band of the single-crystalline Gd_7NiPd_2 and Gd_7Pd_3 (together with the Gd 4f and Gd 5p states) are collected in Fig. 3. The valence band spectrum shows a narrowing and moving away of the Pd 4d states from the Fermi level (full width at half maximum Γ_{FWHM} = 1.4 eV, binding energy BE = 3.7 eV) in comparison with elemental Pd (Γ_{FWHM} = 4.1 eV, BE = 0.95 eV). It is due to a reduction of overlap of the Pd 4d orbitals of the neighbouring Pd atoms in the compound. After substitution of nickel into palladium sublattice the decrease of the intensity of the Pd 4d after normalization to the maximum intensity of Gd 4f is observed. The Pd 4d states are well separated from the Gd 5d ones which form a shoulder at the Fermi level. The Ni 3d stronger overlaps the Gd 5d states than Pd 4d. Hence the Gd 5d states may hybridize with the Ni 3d states considerably larger than with the Pd 4d states. A small decrease of the intensity of Gd 5d line is observed. It may be connected with decreasing number of the d electrons during the substitution of Pd by Ni. Similar behaviour for $Gd_{7-x}Y_xPd_3$ series was observed [5–9].

The XPS spectra of the Pd 3d are shifted by 1.5 eV in relation to pure Pd metal towards the higher binding energy in similar way to other Pd-based compounds of Gd (Fig. 4). Moreover, the Pd 3d lines are symmetric. This confirms the stronger localization character just for the palladium-based compound.

Table 2
Atomic coordinates, isotropic and anisotropic parameters (Å^2) for Gd_7NiPd_2.

Atom	Wyckoff site	x	y	z	$U_{(eq)}$
Gd1	2b	0.66667	0.33333	0.05819(16)	0.01375(18)
Gd2	6c	0.87480(3)	0.12520(3)	0.25255(9)	0.01436(14)
Gd3	6c	0.45990(3)	0.54010(3)	0.05599(8)	0.01450(14)
Pd, Ni	6c	0.18953(6)	0.81047(6)	0.31810(19)	0.01590(18)

Atom	U_{11}	U_{22}	U_{33}	U_{23}	U_{13}	U_{12}
Gd1	0.01423(24)	0.01423(24)	0.01280(37)	0.00000	0.00000	0.00711(12)
Gd2	0.01390(19)	0.01390(19)	0.01511(27)	0.00009(10)	−0.00009(10)	0.00683(17)
Gd3	0.01579(18)	0.01579(18)	0.01208(24)	0.00013(10)	−0.00013(10)	0.00801(17)
Pd, Ni	0.01659(29)	0.01659(29)	0.01790(44)	−0.00131(17)	0.00131(17)	0.01084(34)

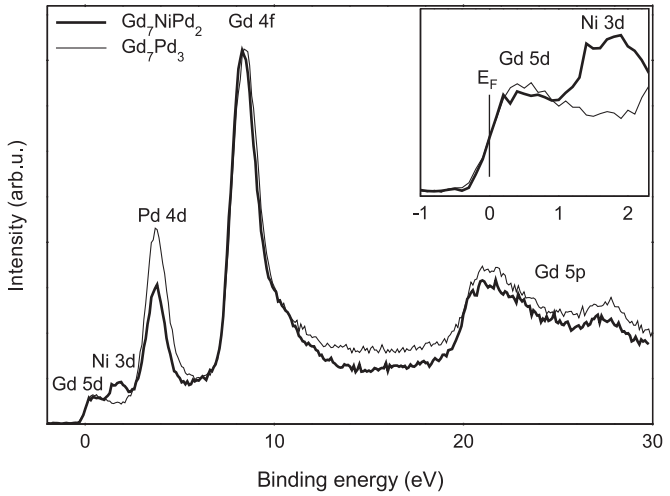

Fig. 3. XPS valence band of the Gd_7Pd_3 and Gd_7NiPd_2 compounds with the Gd 4*f* and Gd 5*p* states.

The Ni 2*p* core level spectra for Gd_7NiPd_2 compound is presented in Fig. 5. In the figure, the result for pure Ni is included for comparison. The spectrum is normalized to the maximum intensity of Ni $2p_{3/2}$ peak. In the investigated sample, the satellite lines are observed but their intensity is much smaller than for pure Ni. This behaviour can be correlated with the hybridization between the Ni 3*d* states and Gd 5*d* states. A similar behaviour was previously observed for $Gd(Ni_{1-x}Co_x)_3$ [12].

The X-ray photoemission spectrum of the Gd 4*d* core level for the Gd_7NiPd_2 compound is shown in Fig. 6. A complex shape of

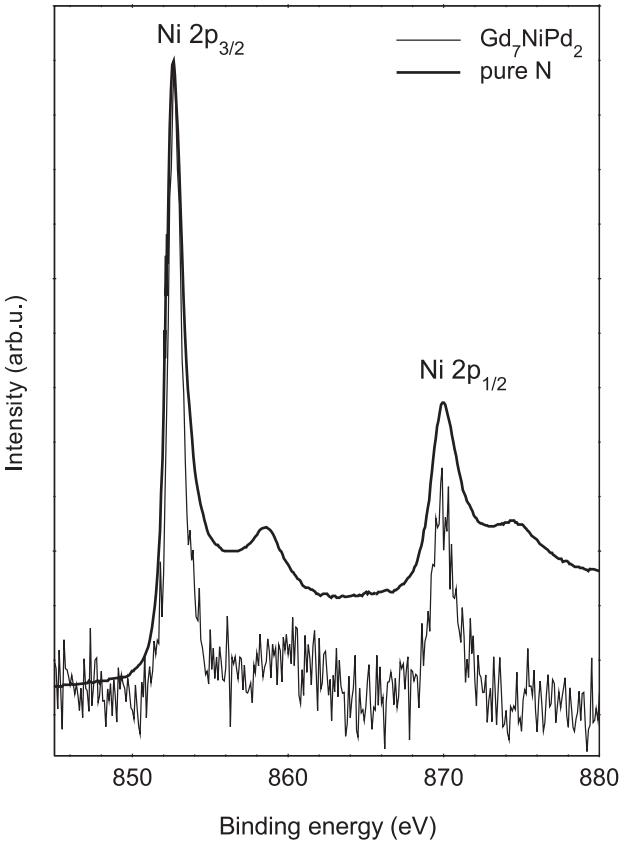

Fig. 5. The Ni $2p_{3/2}$ and $2p_{1/2}$ lines for Gd_7NiPd_2.

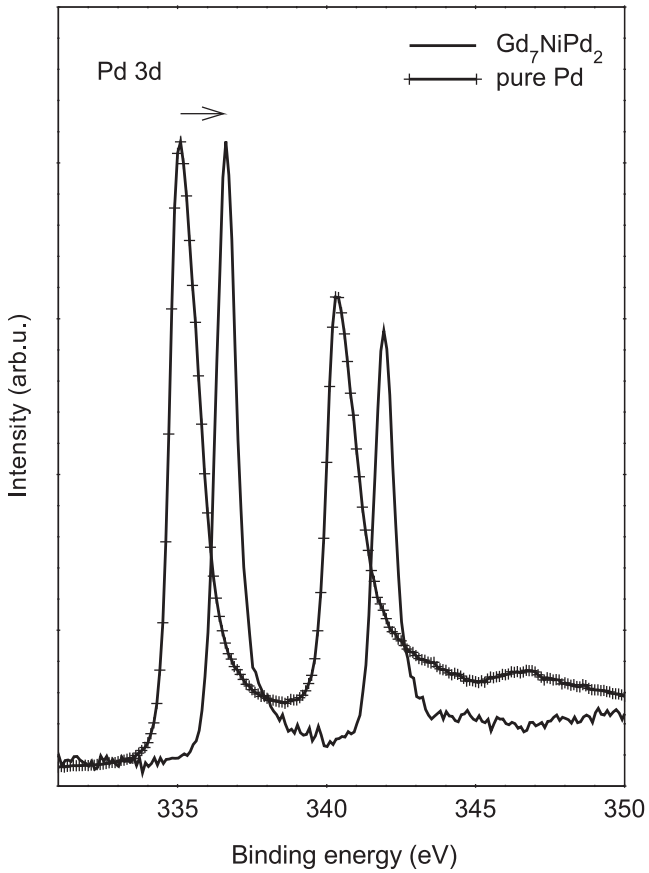

Fig. 4. XPS 3*d* states for pure Pd metal and Gd_7NiPd_2.

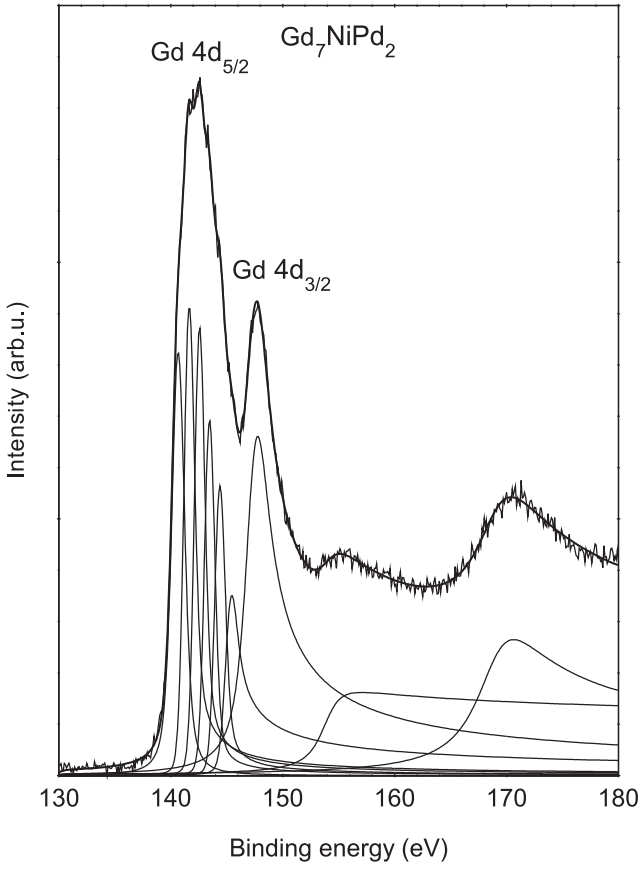

Fig. 6. The deconvoluted XPS of Gd 4*d* states for Gd_7NiPd_2.

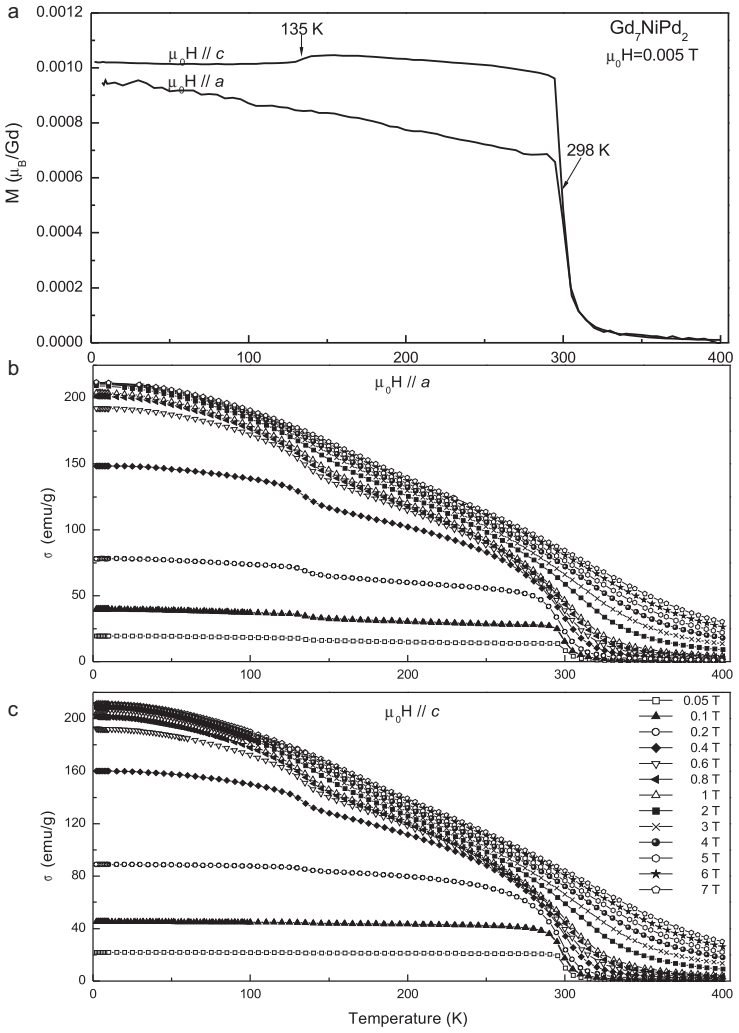

Fig. 7. (a) Temperature dependence of magnetization measured at 5 mT. (b and c) Magnetization versus temperature for different magnetic fields along the principal directions.

the Gd 4*d* line is caused by strong 4*d*–4*f* Coulomb, exchange and spin–orbit interactions. As can be seen in Fig. 6 two main peaks separated by about 5 eV, due to spin–orbit interactions, corresponding to the doublets Gd $4d_{5/2}$ and $4d_{3/2}$ occur. The first peak corresponds to mainly ^{9}D final states while the further peaks of the spectrum have mainly ^{7}D character. The first peak exhibits additional multiplet structure. The 4*d*–4*f* (super-Coster–Kronig) decay process in the final state is mainly responsible for the broadening and the additional splitting of the spectrum (especially visible for Gd $4d_{5/2}$).

Fig. 7a shows the temperature dependence of the magnetization for Gd_7NiPd_2; with a measuring magnetic field equal to 5 mT along the principal directions. Below 325 K, the magnetization for μ_0H//*a*- and μ_0H//*c*-axes rapidly increases due to a ferromagnetic-type order of the Gd sublattice. Besides the magnetic phase transition at 298 K an additionally transition for the *c* direction below the ordering temperature is observed. We interpret this anomaly as due to a reorientation of the Gd-spins.

Fig. 7c and d shows magnetization *M*(T) measured in the magnetic fields 0.01–7 T. The observed changes in magnetization runs show the alignment of the magnetic moment with growing magnetic field.

The reorientation processes are confirmed by the real *ac*-susceptibility data (Fig. 8). In the imaginary part of *ac* susceptibility after transition at 298 K a minimum is observed. This may be

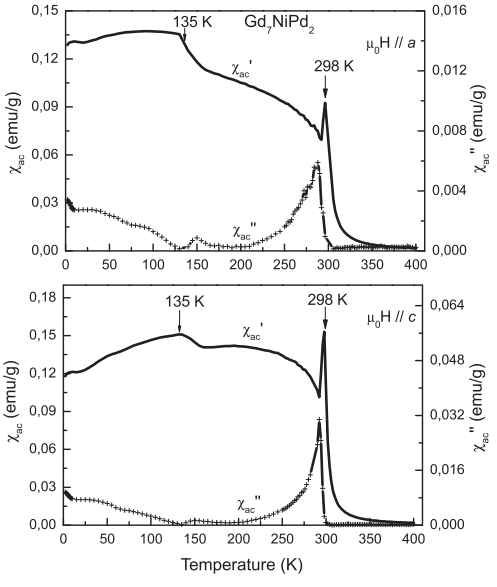

Fig. 8. Temperature dependence of real and imaginary parts of *ac* magnetic susceptibility of Gd_7NiPd_2 at 100 Hz.

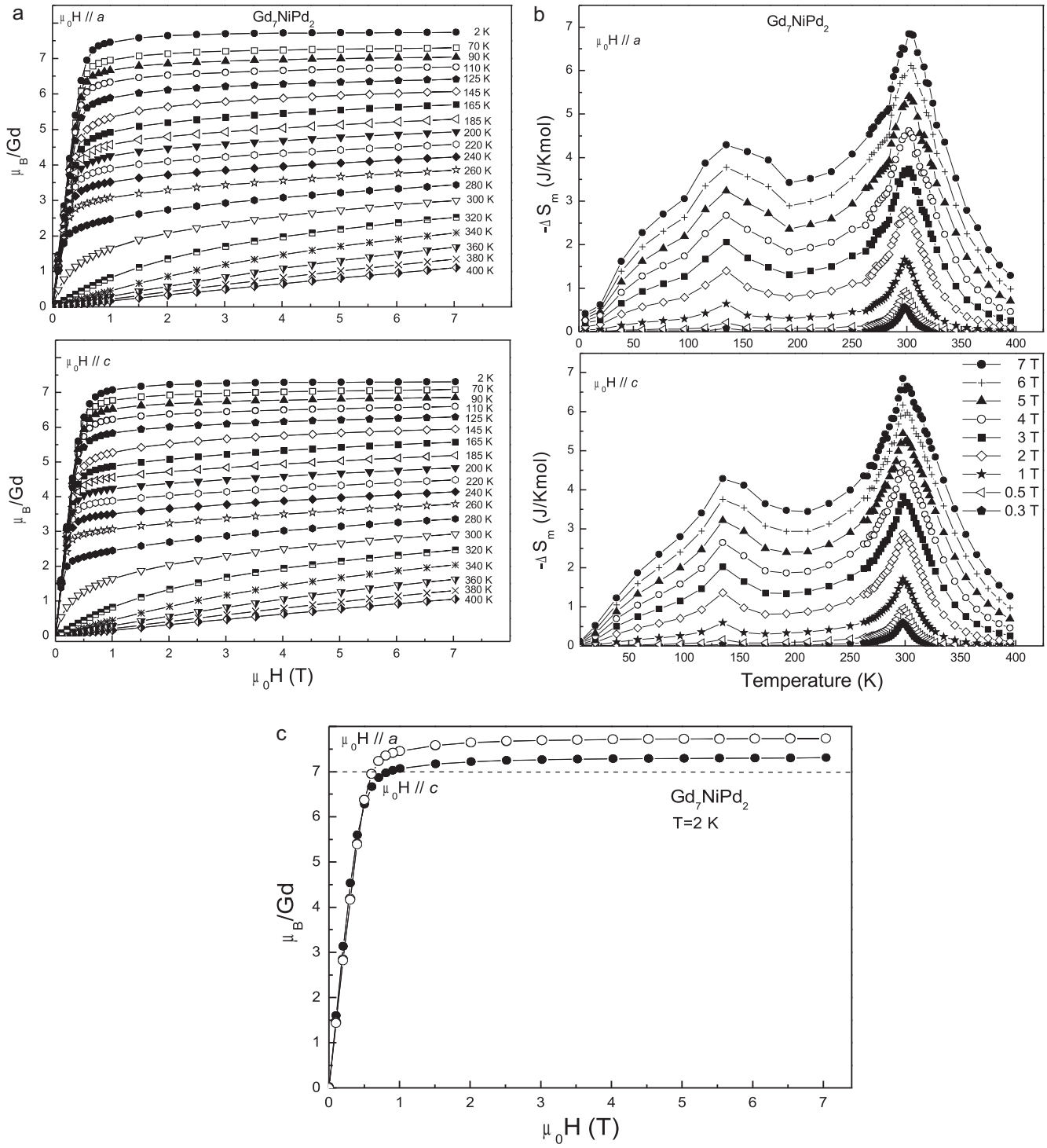

Fig. 9. (a) Magnetization versus magnetic fields along the principal directions. (b) Calculated entropy change for different magnetic field variations. (c) Magnetization in magnetic fields applied parallel to *a*- and *c*-axes at 2 K for Gd_7NiPd_2.

attributed to the established ferromagnetic like arrangement of the magnetic moment. Then, below 135 K the increase of the χ_{ac}''(T) susceptibility value and the peaks related to the reorientation process occur. The peaks in the imaginary part are connected with energy dissipation during the reorientation process. This observation could support an antiferromagnetic tendency of the spin orientation in lower temperatures. A similar behaviour was previously observed for $Gd_5Y_2Pd_3$, $Gd_4Y_3Pd_3$ and $Gd_3Y_4Pd_3$ [7–9].

Fig. 9a shows the isotherm magnetization curves measured along *a*- and *c*-axes. A nonlinear behaviour of the isotherms above transition temperature (T_C = 289 K) is observed. This may be attributed to the short range correlations above the ordering temperature or due to the palladium *d* band contribution.

Fig. 9b presents the temperature dependence of the entropy change, ΔS_m, for different magnetic field variations for the Gd_7NiPd_2. The calculations of the magnetic entropy change were performed using the isothermal magnetization curves $M(H)$. The

variation of magnetic entropy and $M(H)$ isotherms are related by the thermodynamic Maxwell relation [13]:

$$\left(\frac{\partial S}{\partial H}\right)_T = \left(\frac{\partial M}{\partial T}\right)_H. \quad (1)$$

From Eq. (1) the isothermal entropy change can be calculated by means of magnetic measurements:

$$\Delta S_M(T,H) = S_M(T,H) - S_M(T,0) = \int_0^H \left(\frac{\partial M}{\partial T}\right)_{H'} dH'. \quad (2)$$

For magnetization measurements made at discrete field and different temperatures, Eq. (2) can be approximated by [14]:

$$\left|\Delta S_M\right| = \sum_i \frac{(M_i - M_{i+1})_H}{T_{i+1} - T_i} \Delta H_i, \quad (3)$$

where M_i and M_{i+1} represent the magnetization values measured in a field H, at temperatures T_i and T_{i+1}, respectively.

The maximum value of the entropy change is located near the magnetic transition temperature of the compound, (T_C = 298 K). It is also clear visible that the MCE increases with the increase of applied magnetic field. The maximum entropy change value amounts −2.79 J/K kg for *a*-axis and −2.87 for *c*-axis, −5.22 J/K kg for *a*-axis and −5.44 J/K kg for *c*-axis and −6.85 J/K kg for *a*-axis and −6.49 J/K kg for *c*-axis, respectively at 2, 5 and 7 T.

The magnetization of Gd_7NiPd_2 in magnetic field applied parallel to *a*- and *c*-axes at 2 K shown Fig. 9c. The saturation moments values per gadolinium atom exceed that expected for the free Gd^{3+} ions of gJ = 7 μ_B and equal 7.73 μ_B for *a*-axis and 7.31 μ_B for *c*-axis. We attribute this behaviour to an itinerant electron contribution of the conduction band associated with 3*d* states of the Ni ions, 4*d* states of the Pd ions together with 5*d* states of the Gd ions. The contribution of both 4*d* and 5*d*-bands is documented by XPS data shown above, where these bands are found to locate near the Fermi level. Moreover, the Compton scattering research of Gd_7Pd_3 confirmed that the 4*d*-Pd and 5*d*-Gd bands give a sizable contribution to the total spin moment [15]. The value of the saturation moment is greater for H//*a* in compare to H//*c*. Such behaviour for the Gd_7Pd_3, Gd_4Y_3Pd3 and $Gd_3Y_4Pd_3$ compounds was earlier observed [5–9].

4. Conclusion

The crystal and electronic structure, *ac*-magnetic susceptibility, *dc*-magnetization and magnetocaloric properties of Gd_7NiPd_2 single crystal was measured. The Gd ions in their magnetic sublattice possess a large and localized magnetic moment. Therefore, the exchange interactions between Gd ions are a dominating mechanism being responsible for the ordering in the studied compound. However, an induced magnetic moment of metal *T* may modify these interactions leading to different ordering temperatures depending on a value of the induced moment. So that the influence of the *T* sublattice is not negligible and can cause some changing or modulation in the long-range (RKKY) exchange interactions and magnitudes of the ordering temperature. Moreover, for the Gd_7Pd_3 a stronger localization of the Pd 4*d* states is observed. In the Gd_7NiPd_2 compound between Gd 5*d* and Pd 4*d* states the Ni 3*d* band is localized. Thus in Gd_7NiPd_2 compound the *d* electrons have bigger share in the density of states at the Fermi energy than that of the d electrons in Gd_7Pd_3. The recent investigations of the GdPdX (X = Al, Si, Ge, Ga and Sn) systems [16] or GdNiAl, GdCuAl [17,18] showed the tendency of increasing ordering temperature with increasing the distance of the d states from the Fermi level. All GdPdX (X = Al, Si, Ge, Ga and Sn) compounds crystallizing in the orthorhombic crystal structure have the ordering temperatures very close to one another which amount around 30 K, while for GdPdIn the ordering temperature was as high as 110 K. For the latter compound the stronger localization of the Pd 4*d* electrons was found from the electronic structure measurements [16]. For other GdPdX compounds the Pd 4*d* states are more overlapped with the Gd 5*d* states. Thus a strong localization of the d states of the transition metal causes negligible influence on the exchange interactions in the Gd sublattice.

The observed transitions at 298 and 135 K are interpreted as the ferromagnetic-type ordering and spin-reorientation, respectively. Moreover, an enhancement of the magnetic moments of Gd^{3+} is observed. This behaviour may be ascribed to the itinerant electron contribution associated with 3*d* of Ni ions, 4*d* of Pd ions together with 5*d* of Gd ones.

The Gd_7NiPd_2 compound exhibits ordering temperature near room temperature and the half-height width of the MCE peaks are large enough in order to be used as an active magnetic refrigerator in a wide range of the temperature. Moreover, the Gd_7NiPd_2 exhibit similar values of the magnetocaloric effect like Gd_7Pd_3 [19] and the substitution of nickel atom into palladium position decreasing costs of the compound. Therefore, the Gd_7NiPd_2 belongs to the class of promising materials with high magnetocaloric effect.

References

[1] V.K. Pecharsky, K.A. Gschneidner Jr., Int. J. Refrig. 29 (2006) 1239.
[2] K.A. Gschneidner Jr., V.K. Pecharsk, A.O. Tsokol, Rep. Prog. Phys. 68 (2005) 1479.
[3] D.T. Cam Thanh, E. Brück, O. Tegus, J.C.P. Klaasse, K.H.J. Buschow, J. Magn. Magn. Mater. 310 (2007) e1012.
[4] E. Brück E., J. Phys. D: Appl. Phys. 38 (2005) R381.
[5] E. Talik, M. Klimczak, R. Troć, J. Kusz, W. Hofmeister, A. Damm, J. Alloys Compd. 427 (2007) 30.
[6] E. Talik, M. Klimczak, R. Troć, J. Kusz, W. Hofmeister, A. Winiarski, J. Alloys Compd. 460 (2008) 1.
[7] E. Talik, M. Klimczak, A. Winiarski, R. Troć, J. Crystal Growth 310 (2008) 1886.
[8] E. Talik, M. Klimczak, V.H. Tran, J. Kusz, W. Hofmeister, A. Winiarski, R. Troć, Intermetallics 10 (2010) 27.
[9] E. Talik, M. Oboz, V.H. Tran, J. Kusz, W. Hofmeister, A. Winiarski, J. Crystal Growth 312 (2010) 1651.
[10] E. Talik, J. Szade, J. Heimann, A. Winiarska, J. Winiarski, A. Chełkowski, J. Less-Common Met. 138 (1988) 129.
[11] G.M. Sheldrick, SHELX-97, Program for crystal structure refinement, University of Göttinge, Germany, 1997.
[12] M. Kwiecień, G. Chełkowska, K. Rabijasz, J. Alloys Compd. 423 (2006) 55.
[13] H.B. Callen, Thermodynamics, Wiley, New York, 1981 (Chapter 14).
[14] M. Földeàki, R. Chahine, T.K. Bose, J. Appl. Phys. 77 (1995) 3528.
[15] C. Shenton-Taylor, J.A. Duffy, J.W. Taylor, C.A. Steer, D.N. Timms, M.J. Cooper, L.V. Blaauw, J. Phys. Condens. Matter 19 (2007) 186208.
[16] E. Talik, J. Kusz, W. Hofmeister, M. Matlak, M. Skutecka, M. Klimczak, J. Alloys Compd. 423 (2006) 47.
[17] J. Jarosz, E. Talik, T. Mydlarz, J. Kusz, H. B¨ohm, A. Winiarski, J. Magn. Magn. Mater. 208 (2000) 169.
[18] G. Ehlers, H. Maletta, Z. Phys. B 99 (1996) 145.
[19] F. Canepa, M. Napoletano, S. Cirafici, Intermetallics 10 (2002) 731.